Evaluation of Reinforcement Strain Growth During Traffic Loading

by

Steve Perkins
Associate Professor
Department of Civil Engineering

Western Transportation Institute
Montana State University

A report prepared for the

Western Transportation Institute
University Transportation Center

April 20, 2005

DISCLAIMER

The opinions, findings and conclusions expressed in this publication are those of the authors and not necessarily those of Montana State University.

Alternative accessible formats of this document will be provided upon request. Persons with disabilities who need an alternative accessible format of this information, or who require some other reasonable accommodation to participate, should contact Kate Heidkamp, Communications and Information Systems Manager, Western Transportation Institute, Montana State University-Bozeman, PO Box 173910, Bozeman, MT 59717-3910, telephone number 406-994-7018, e-mail: KateL@coe.montana.edu.

ACKNOWLEDMENTS

The author acknowledges the Montana Department of Transportation, the Federal Highway Administration, the Amoco Fabrics and Fibers Company, Colbond, Inc., Synthetic Industries, Ten Cate Nicolon, Tenax Corporation and Tensar Earth Technologies, Incorporated for the support of projects referenced in this report that provided data used for this project.

The author also acknowledges the research partners who participated on previous projects leading to this report. These partners include: Gudund Eiksund, Geir Svanø and Arnstein Watn of SINTEF Civil and Environmental Engineering, Trondheim Norway, Barry Christopher of Christopher and Associates, Eli Cuelho of the Western Transportation Institute and Chuck Schwartz of the University of Maryland.

TABLE OF CONTENTS

List of Tables

List of Figures

Executive Summary

A recently completed project for the FHWA (Perkins et al. 2004) used the ratio of permanent to resilient (dynamic) geosynthetic strain observed in test sections to establish a growth relationship of this ratio with pavement load cycles to determine the effect of confinement of the reinforcement on the base aggregate layer through restraining shear stresses created between the reinforcement and the base. Geosynthetics showing a faster growth of reinforcement strain ratio with normalized pavement load applications resulted in larger levels of confinement of the base. Within the context of a mechanistic analysis, this procedure provided a means of assessing the stiffness of the base at different periods of pavement life and was used with pavement damage models for rutting to determine the effect of the reinforcement on rutting. In the course of this completed project, data from 3 test sections were evaluated.

In this UTC project, reinforcement strain data from approximately 18 additional large-scale laboratory and field-scale HVS test sections previously reported by Perkins (1999, 2002) are evaluated. These test sections involved the use of different aggregates, subgrades and geosynthetic materials. Several sections were constructed using the same geosynthetic but with different aggregates and with a different thickness of aggregate. Permanent to resilient strain ratio data were compared by plotting this data against a normalized and shifted load cycle number.

In general, the data presented in this report suggests that of the variables incorporated in the test sections (geosynthetic type, subgrade strength, aggregate type, aggregate thickness) only geosynthetic type influences the shape of the normalized curve. The shift value of the normalized curve appears to be dependent on the number of load cycles the pavement can carry before reaching 25 mm of permanent surface deformation, which in turn most likely accounts for variables such as subgrade strength, aggregate type and aggregate thickness. The differences in curve shape between the different geosynthetic types is not as distinct as expected and more work is needed to improve strain measuring techniques to improve this situation.

1. INTRODUCTION

Through projects recently performed for MDT and FHWA, (Perkins, 2002, 1999) geosynthetics have been shown to provide significant benefits in extending the life of flexible pavements when used as reinforcement in the base aggregate layer. A recently completed project for the FHWA (Perkins et al. 2004) focused on the development of mechanistic-empirical design methods for geosynthetic base-reinforced pavements where these methods are compatible with procedures developed under NCHRP Project 1-37a (NCHRP 2004). In the modeling project completed for FHWA (Perkins et al. 2004) data was used from strain gauges attached to three geosynthetic products (two geogrids and one geotextile) used in large-scale laboratory test sections constructed under a project for MDT and reported by Perkins (1999). Permanent and dynamic strain data was evaluated from three test sections for different levels of applied cyclic pavement loads. These experimental results showed the ratio of permanent to dynamic reinforcement strain to increase with increasing pavement load applications.

The growth relationship of the reinforcement strain ratio with pavement load cycles was used to determine the effect of confinement of the reinforcement on the base aggregate layer through restraining shear stresses created between the reinforcement and the base. The relationship established between confinement and reinforcement strain ratio provided a means of predicting the increase in confinement level with an increase in the number of pavement load applications. Geosynthetics showing a faster growth of reinforcement strain ratio with normalized pavement load applications resulted in larger levels of confinement of the base. Within the context of a mechanistic analysis, this procedure provided a means of assessing the stiffness of the base at different periods of pavement life and was used with pavement damage models for rutting to determine the effect of the reinforcement on rutting. This procedure, along with other components of the method developed, showed favorable predictions of the design method to rutting results from large-scale laboratory and full-scale test sections loaded by a heavy vehicle simulator (HVS).

The growth relationship between reinforcement strain ratio and pavement load applications is a critical component of the design process developed. This relationship was evaluated for three geosynthetics in three large-scale laboratory test sections and gave reasonable relationships that provided good predictions of pavement rutting. In this UTC project, reinforcement strain data from approximately 18 additional large-scale laboratory and field-scale HVS test sections previously reported by Perkins (1999, 2002) are evaluated. The test sections reported by Perkins (1999, 2002) involved the use of different aggregates, subgrades and geosynthetic materials. Several sections were constructed using the same geosynthetic but with different aggregates and with a different thickness of aggregate. Evaluation of this data will allow conclusions to be made on the following:

1. Is the relationship between reinforcement strain ratio and normalized pavement load applications unique for any aggregate type and pavement cross section geometry?
2. Are the relationships between reinforcement strain ratio and normalized pavement load applications for different geosynthetics distinct and consistent with the reinforcement benefit seen from these test sections?

The conclusion made for the first question will indicate whether specific measurements of this empirical relationship are needed for different aggregate types and thickness. The conclusion to the second question will indicate the level of data scatter seen with these measurements and

the level of confidence that can be placed on any given measurement set. This in turn will point to whether generic relationships should be used for different classes of geosynthetics as opposed to product specific relationships.

This information is needed before the methods developed in the project for FHWA (Perkins et al., 2004) can ultimately be implemented as an addendum to the future AASHTO Guide. When an NCHRP project is formed to perform this implementation, all background research involving the development of design and testing methods will need to be completed such that implementation is performed with off-the-shelf research.

2. METHODOLOGY

The approach used in this project was to reduce geosynthetic strain data from two previous projects (Perkins, 2002, 1999) by plotting the dynamic strain, permanent strain and the ratio of permanent to dynamic strain versus normalized load cycle applications. Data from all available test sections were used, provided the data was free of obvious instrumentation failures. This data is examined and used to draw conclusions on whether the relationships observed are dependent on variables incorporated in the test sections, which include geosynthetic type, base aggregate type, subgrade type, and base aggregate thickness.

3. BACKGROUND

Experimental and theoretical studies on reinforcement of aggregate base layers in flexible pavements using geosynthetics have shown that the principal effect of the reinforcement is to provide lateral confinement of the aggregate (Bender and Barenberg, 1978; Kinney and Barenberg, 1982; Perkins 1999; Perkins and Edens, 2002). Lateral confinement is due to the development of interface shear stresses between the aggregate and the reinforcement, which in turn transfers load to the reinforcement. As a cycle of traffic load is applied, there is both a resilient or recoverable shear stress and a permanent shear stress that exists when the traffic load is removed. The permanent interface shear stress continues to grow as repeated traffic loads are applied, meaning that the lateral confinement of the aggregate base layer becomes greater with increasing traffic load repetitions.

The reinforced pavement response model developed by Perkins et al. (2004) was formulated to account for the effect of increasing lateral confinement with increasing traffic load repetitions. This response model uses a relationship between increasing permanent interface shear stress and traffic pass level developed in this section. This relationship is obtained from field data by examining tensile strains developed in the reinforcement as a function of traffic passes and relating this development to interface shear stress through appropriate theoretical considerations.

3.1. Field Data

Previously reported test sections (Perkins 1999) showed the development of extensional horizontal strain at the bottom of the base aggregate layer under the area of the load, as shown for a typical test section in Figure 1, where extensional strain is taken as positive. The magnitude of strain is seen to increase with increasing traffic load repetitions. Relative motion is created between the aggregate and the relatively stiff reinforcement, which in turn creates interface shear stress. This shear stress induces load and strain in the reinforcement with the reinforcement strain distribution shown in Figure 2 for a typical test section and where tensile strain is taken as positive. The observation of both a permanent lateral strain in the aggregate layer and a permanent strain in the reinforcement, which both grow with applied traffic cycles, indicates the presence of a permanent interface shear stress.

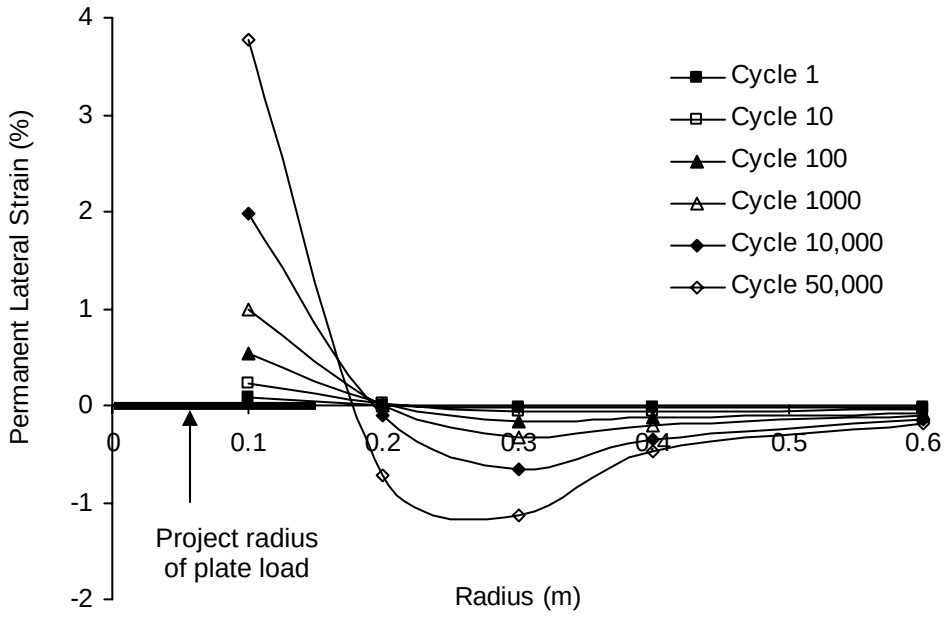

Figure 1: Development of lateral strain in the bottom of a base aggregate layer with traffic load repetitions.

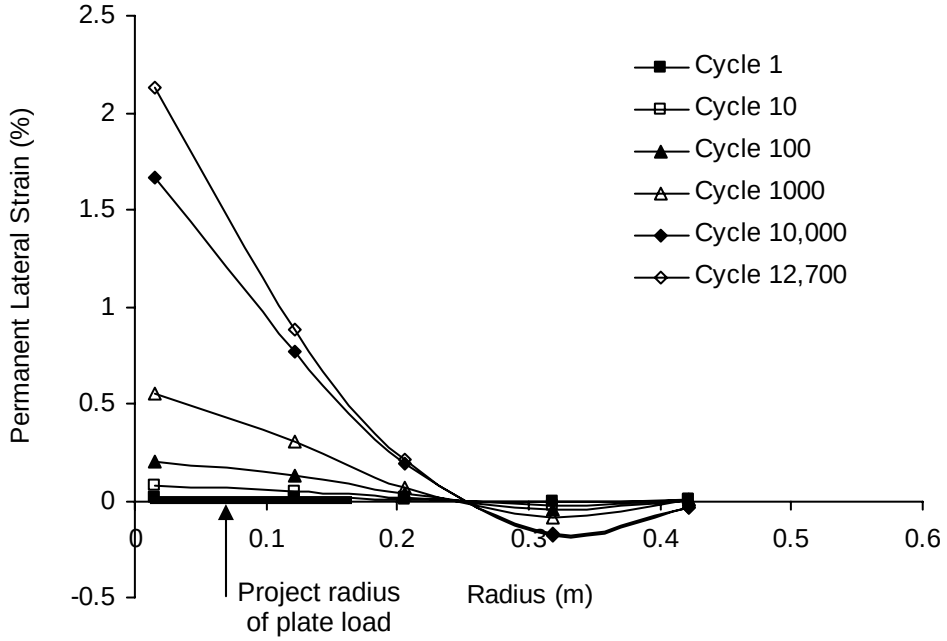

Figure 2: Development of lateral strain in a reinforcement layer with traffic load repetitions.

3.2. Theory

In order to relate measured reinforcement strain to interface shear stress, an infinitesimal axisymmetric element of the reinforcement is considered (Figure 3). The interface shear stress from relative movement of the base is considered as a unit shear stress, τ. Force equilibrium in the radial direction for an infinitesimal element having a thickness of dt is given by Equation (1).

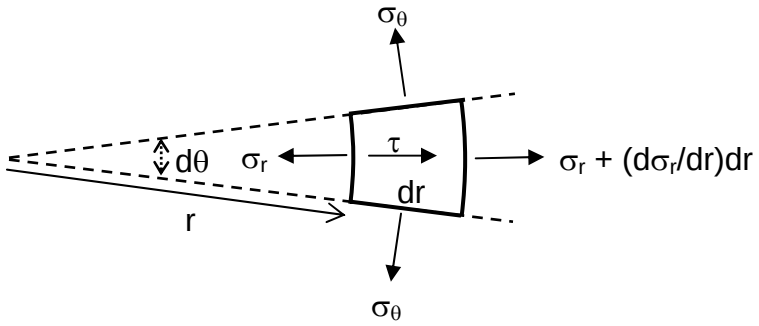

Figure 3: Infinitesimal reinforcement element.

$$\frac{d\sigma_r}{dr} r\,dr\,d\theta\,dt + \sigma_r\,dr\,d\theta\,dt + \tau\,r\,dr\,d\theta\,dt - \sigma_\theta\,dr\,d\theta\,dt = 0 \quad (1)$$

Dividing Equation by rdrdθdt yields Equation (2).

$$\frac{d\sigma_r}{dr} + \frac{\sigma_r - \sigma_\theta}{r} + \tau = 0 \quad (2)$$

If it assumed that the difference in stresses between the radial and the ring directions is small, such as in the vicinity of the centerline of the test section, Equation (2) can be approximated by Equation (3). Since the majority of the reinforcement effect arises from an area centered under the wheel load, Equation (3) is used for the entire radius of the model.

$$\frac{d\sigma_r}{dr} + \tau = 0 \quad (3)$$

Separating and integrating Equation (3) produces Equation (4).

$$\sigma_r = \int \tau\, dr \quad (4)$$

If the reinforcement is assumed to correspond to an elastic material with an elastic modulus in any principal direction given by E, then the stress σ_r can be replaced by εE, where ε is the strain in the reinforcement in the radial direction. Equation (4) can then be expressed in terms of strain for the dynamic (resilient) state, ε_r, when a resilient interface shear stress, τ_r, acts on the reinforcement (Equation (5)) and for the state when locked-in or permanent strain, ε_p, exists in

the reinforcement when the pavement load is removed and a locked-in or permanent shear stress, τ_p, acts on the reinforcement (Equation (6)).

$$\varepsilon_{\mathrm{r}} = \frac{\int \tau_r \, dr}{E} \tag{5}$$

$$\varepsilon_{\mathrm{p}} = \frac{\int \tau_p \, dr}{E} \tag{6}$$

If it is assumed that the shape of the functions for τ_r and τ_p are identical, then Equations (5) and (6) can be combined to yield Equation (7).

$$\tau_{\mathrm{p}} = \tau_r \frac{\varepsilon_p}{\varepsilon_r} \tag{7}$$

Provided the permanent to resilient reinforcement strain ratio ($\varepsilon_p/\varepsilon_r$) and the resilient interface shear stress, τ_r, can be determined, Equation (7) allows for the permanent interface shear stress, τ_p, to be calculated. The focus of the work performed for this project was in determining $\varepsilon_p/\varepsilon_r$ from experimental test section data. The resilient interface shear stress, τ_r, is determined from pavement response models as described by Perkins et al. (2004).

4. TEST SECTION DATA

4.1. Test Sections Evaluated

Test sections constructed under two projects where geosynthetics were instrumented with strain gauges are used in this study. The first project (Perkins 1999) used a pavement test facility consisting of a concrete box (2 m × 2 m × 1.5 m in height) in which pavement layers (subgrade, geosynthetic, base aggregate and asphalt concrete) were constructed. Cyclic pavement load was applied to a circular plate resting on a waffled rubber pad. The second project used a similar pavement test facility located at GeoTesting Express, Atlanta, Georgia. The second project also included pavement test sections constructed in the CRREL FERF facility that were loaded with a heavy vehicle simulator.

Table 1 provides a description of the variables associated with the test sections available through these two projects. The test sections with the label "MSU" were constructed using the test box located at MSU. The "CS" and "SSS" sections were constructed under the project reported by Perkins (1999). The test sections labeled "T" and "R" were constructed under the project reported by Perkins (2003). The sections labled "GTX" were constructed using the test box at GeoTesting Express and were reported in Perkins (2003). The test sections labeled CRREL were constructed using the facility at CRREL and were also reported in Perkins (2003).

The asphalt concrete, base aggregate and subgrade materials used to construct the test sections are described in detail in the above referenced reports. The asphalt materials were all hot-mix asphalts from various batch plants. The aggregates (with the exception of MSU2) were relatively standard crushed aggregates from local sources. The MSU2 aggregate was a rounded, uncrushed pit run material. The MSU CS subgrade was a high plasticity clay prepared at a water content and dry density to yield a CBR of approximately 1.5. The MSU SSS subgrade was a silty sand with a CBR between 8 to 15. The CRREL/GTX subgrade was a high plasticity clay with a CBR between 1 to 1.5. The geosynthetics used are listed in Table 2.

Table 3 provides notes on test sections containing bad sensors where the data was unusable or other special conditions associated with the tests. The loading in a number of sections was not carried out to a rut depth of 25 mm, meaning that the parameter $N_{25\ mm}$ used to normalize the applied load cycles (as described in the next section) had to be extrapolated from the point at which the test stopped.

Table 1: Details of test sections evaluated.

Section	Layer Thickness (mm)		Layer Types				Geosynthetic Position*
	AC	Base	AC	Base	Subgrade	Geosynthetic	
MSU CS1	75	300	MSU	MSU1	MSU CS	G	1
MSU CS3	75	300	MSU	MSU1	MSU CS	G	2
MSU CS5	75	300	MSU	MSU1	MSU CS	H	1
MSU CS6	75	300	MSU	MSU1	MSU CS	A	1
MSU CS7	75	300	MSU	MSU1	MSU CS	G	2
MSU CS10	75	375	MSU	MSU1	MSU CS	G	1
MSU CS11	75	300	MSU	MSU1	MSU CS	G	1
MSU SSS2	75	200	MSU	MSU1	MSU SSS	G	3
MSU SSS3	75	200	MSU	MSU1	MSU SSS	A	3
MSU SSS5	75	200	MSU	MSU1	MSU SSS	G	1
MSU SSS8	75	200	MSU	MSU1	MSU SSS	A	1
MSU SSS9	75	200	MSU	MSU1	MSU SSS	G	1
MSU T1	75	175	MSU	MSU1	MSU CS	G	1
MSU T2	75	140	MSU	MSU1	MSU CS	H	1
MSU T3	75	140	MSU	MSU1	MSU CS	H	1
MSU T4	75	175	MSU	MSU1	MSU CS	G	1
MSU T5	75	200	MSU	MSU1	MSU CS	A	1
MSU T6	75	175	MSU	MSU1	MSU CS	G	1
MSU T7	75	200	MSU	MSU1	MSU CS	A	1
MSU R2	75	300	MSU	MSU2	MSU CS	A	1
MSU R4	75	300	MSU	MSU2	MSU CS	G	1
MSU R5	75	300	MSU	MSU2	MSU CS	A	1
GTX3	75	300	GTX	GTX	CRREL/GTX	G	1
GTX6	75	300	GTX	GTX	CRREL/GTX	D	1
GTX7	75	300	GTX	GTX	CRREL/GTX	B	1
GTX8	75	300	GTX	GTX	CRREL/GTX	H	1
GTX9	75	300	GTX	GTX	CRREL/GTX	F	1
GTX10	75	300	GTX	GTX	CRREL/GTX	C	1
GTX11	75	300	GTX	GTX	CRREL/GTX	E	1
CRREL2	75	300	CRREL	CRREL	CRREL/GTX	G	1
CRREL3	75	300	CRREL	CRREL	CRREL/GTX	A	1
CRREL4	75	300	CRREL	CRREL	CRREL/GTX	H	1

* 1 = base/subgrade interface; 2 = 100 mm above base/subgrade interface; 3 = 40 mm above base/subgrade interface

Table 2: Geosynthetics used in test sections.

Generic Name	Manufacturer & Brand Name	Geosynthetic Type	Geosynthetic Polymer Type / Structure
Geosynthetic A	Amoco ProPex 2006	Geotextile	Polypropylene / Woven
Geosynthetic B	Colbond Enkagrid Max 20	Geogrid	Polypropylene / Welded grid
Geosynthetic C	Colbond Enkagrid Max X1	Geogrid	Polypropylene / Welded grid
Geosynthetic D	Synthetic Industries Geotex 3×3	Geotextile	Polypropylene / Woven
Geosynthetic E	Ten Cate Nicolon Geolon HP570	Geotextile	Polypropylene / Woven
Geosynthetic F	Tenax MS220b	Geogrid	Polypropylene / Extruded, multi-layer
Geosynthetic G	Tensar BX1100	Geogrid	Polypropylene / Biaxial, punched, drawn
Geosynthetic H	Tensar BX1200	Geogrid	Polypropylene / Biaxial, punched, drawn

4.2. Data Reduction

Resilient (or dynamic) strain (ε_r) and permanent strain (ε_p) data from the strain gauges attached to the geosynthetics in the test sections described above were reduced. Resilient and permanent strain data is defined according to the schematic cyclic data shown in Figure 4. For each test section, data for ε_r and ε_p versus applied load cycle were available. In order to compare data between test sections, this strain data was plotted against a normalized load cycle, defined by the actual applied load cycle (N) divided by the number of load cycles necessary to reach 25 mm of permanent surface deformation ($N_{25\ mm}$). According to this definition, the load cycle ratio ($N/N_{25\ mm}$) varies between a very small number and 1 for tests being concluded when 25 mm of permanent surface deformation is reached.

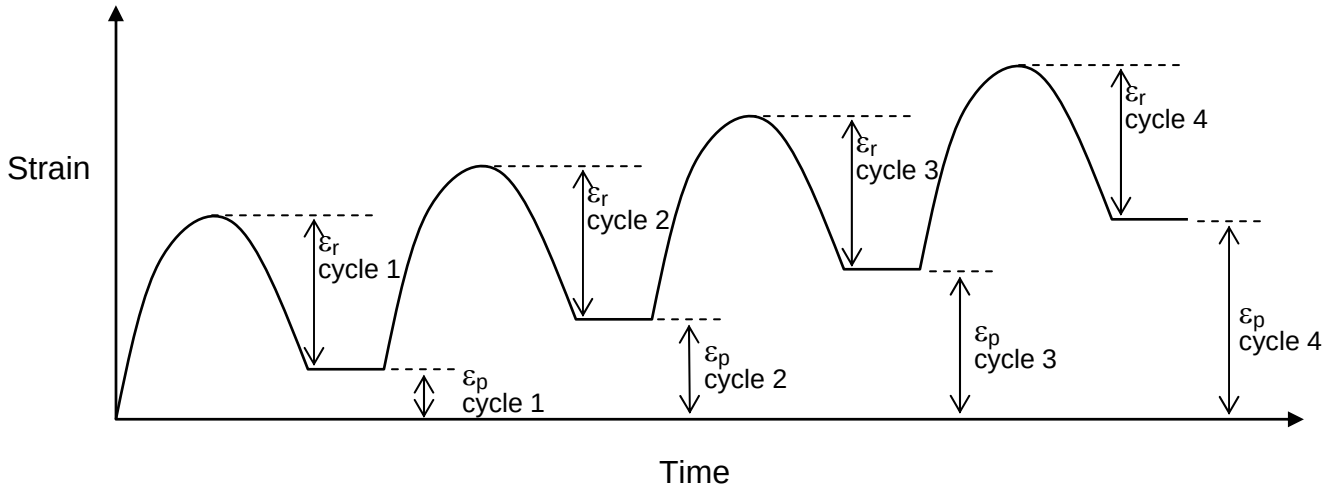

Figure 4: Schematic illustration of cyclic geosynthetic strain data for the definition of resilient and permanent strain.

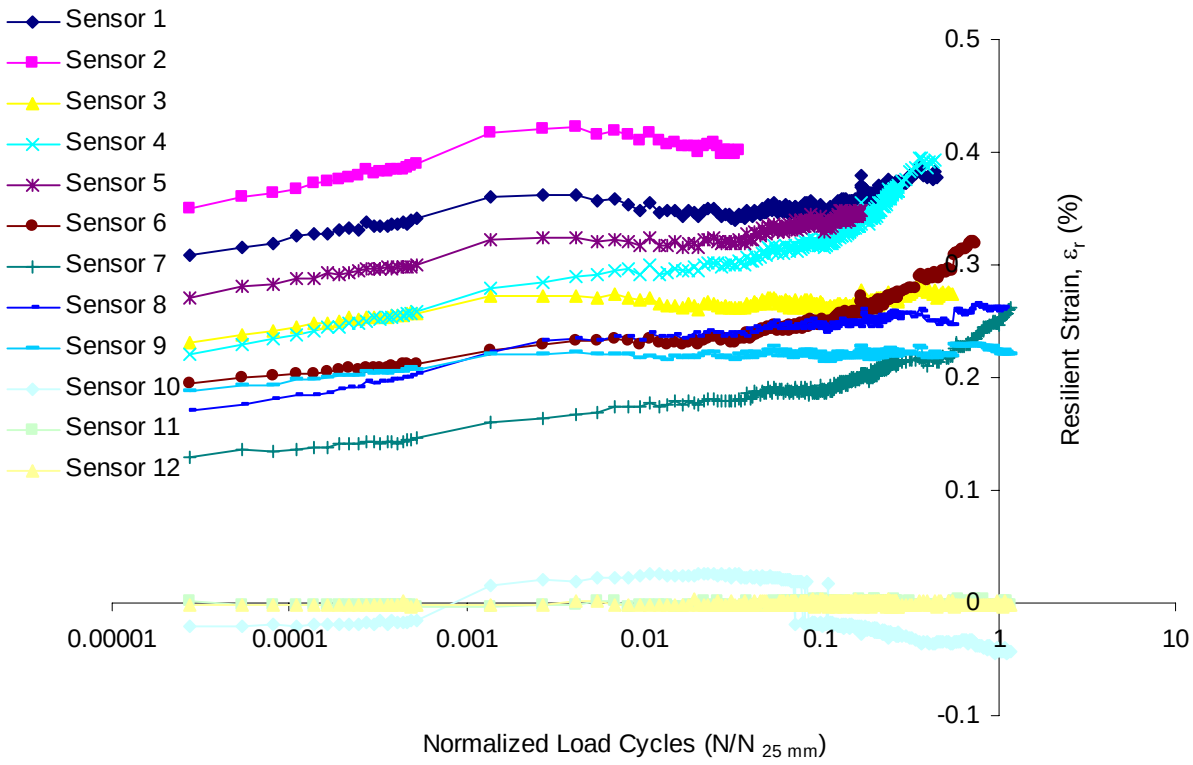

Figure 5: Resilient strain vs. normalized load cycle number, test section CS1

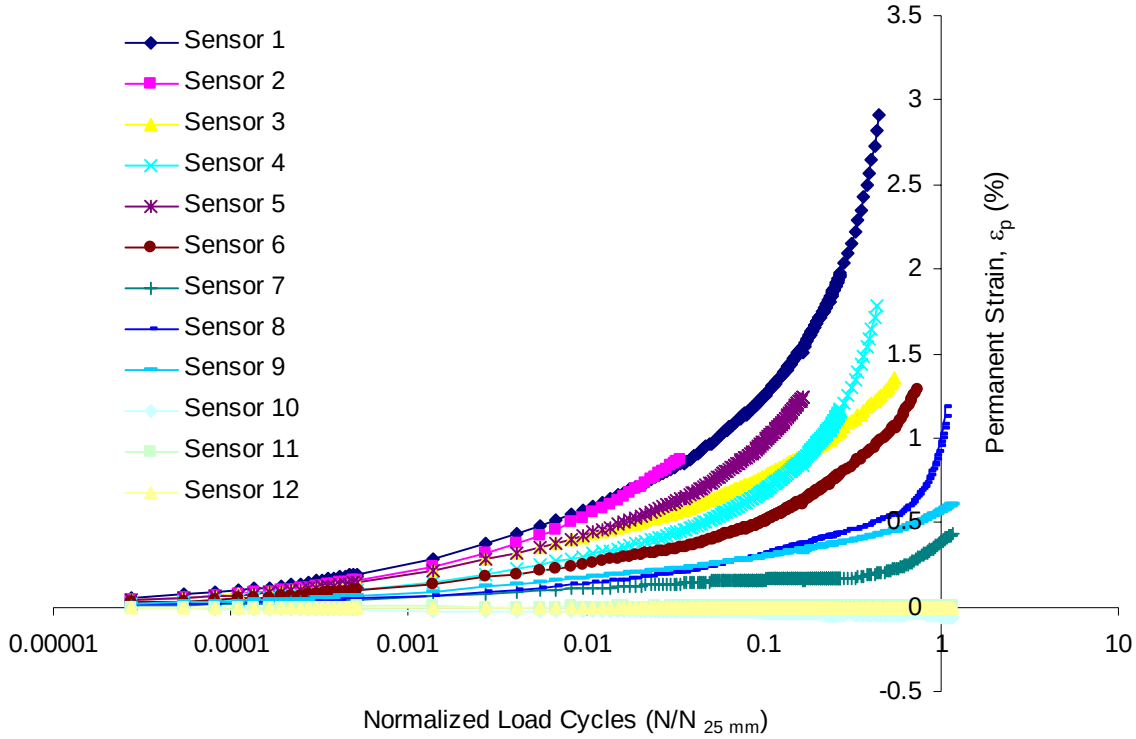

Figure 6: Permanent strain vs. normalized load cycle number, test section CS1

Figure 7 shows data from test section CS1 for 12 strain gauges attached to the geogrid used in this section, where the locations of these gauges are described in Table 4. The gauges were placed to measure strain in either the radial (R) or transverse (T) directions of the material. Figure 5 shows that the resilient strain is relatively constant over the loading period of the pavement. As illustrated in Figure 8, the magnitude of resilient strain decreases with increasing distance from the load plate centerline with small differences between the machine and cross machine directions and with generally larger resilient strain values in the transverse direction of the material. Figures Figure 6 and Figure 7 show similar trends in that permanent strain and the permanent to resilient strain ratio decrease with increasing distance from the load plate centerline with small differences between the machine and cross machine directions and with generally larger values in the transverse direction of the material. Since the assumptions made in the theory described in Section 3.2 pertain to the area centered around the load plate centerline, the focus of the remaining work will be to examine the permanent to resilient strain ratios for the points closest to the load plate centerline.

Table 3 Reinforced Test Section Notes

Section	Comments
MSU CS5	N_{25mm} extrapolated from 17 mm
MSU CS6	N_{25mm} extrapolated from 22 mm
MSU CS7	N_{25mm} extrapolated from 13 mm
MSU CS10	N_{25mm} extrapolated from 17 mm
MSU SSS2	N_{25mm} extrapolated from 22 mm
MSU SSS3	Bad sensors; data not used
MSU SSS5	N_{25mm} extrapolated from 7.4 mm
MSU SSS8	N_{25mm} extrapolated from 8.3 mm
MSU SSS9	N_{25mm} extrapolated from 9.9 mm
MSU T2	Data in M direction only
MSU T5	N_{25mm} extrapolated from 11 mm
MSU T6	Rutting only to 2.7 mm; data not used
MSU T7	N_{25mm} extrapolated from 12 mm
MSU R4	Data in M direction from R=132 mm
MSU R5	Bad sensors; data not used
GTX3	Data in X direction only
GTX6	Data in M direction only and from R=125 mm.
GTX7	N_{25mm} extrapolated from 17 mm.
GTX10	Two loadings; N_{25mm} extrapolated from 13 mm; Data from M direction only and from R=125 mm.
GTX11	Two loadings; Data good only from sensor 6 R=375 mm and not used.
CRREL2	Bad sensors; data not used
CRREL3	Bad sensors; data not used
CRREL4	Bad sensors; data not used

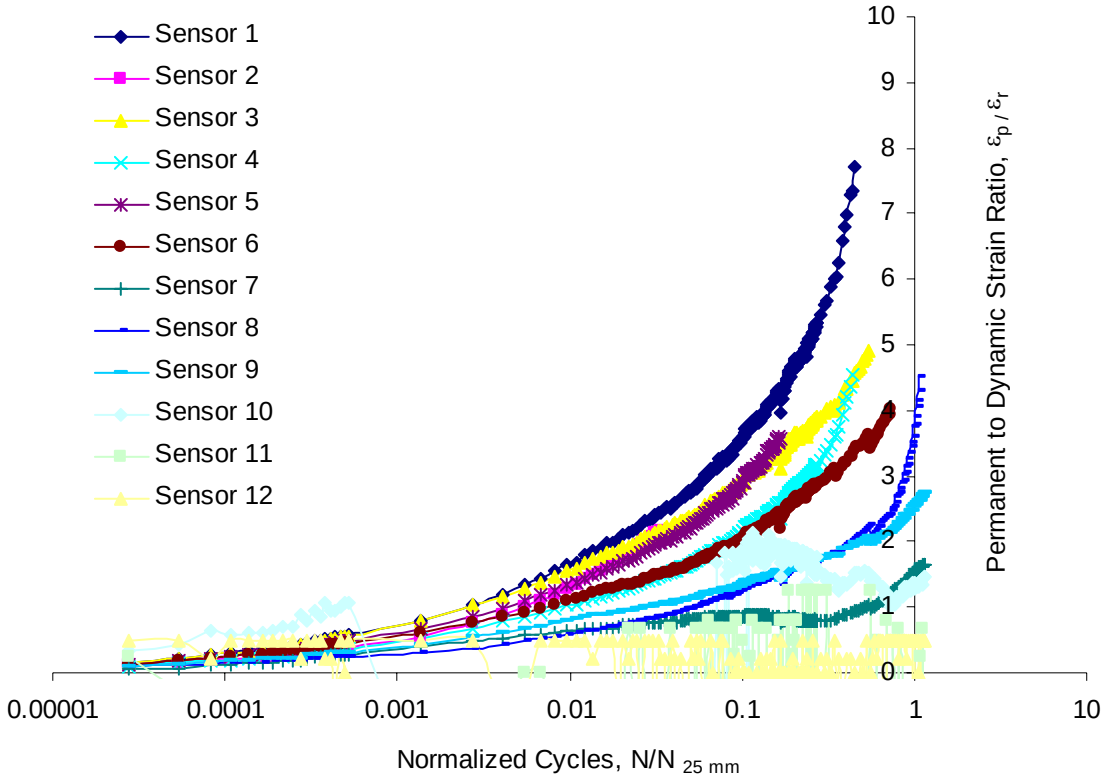

Figure 7: Permanent to resilient strain ratio vs. normalized load cycle number, test section CS1

Table 4: Locations of strain gauges for test section CS1

Gauge	Material Direction	Measurement Direction	x (mm)	y (mm)
1	M	R	15	0
2	X	R	0	23
3	M	T	15	-120
4	M	R	126	0
5	X	T	-114	23
6	X	R	0	140
7	M	R	-215	0
8	X	T	198	-23
9	M	T	-15	315
10	X	R	0	-293
11	X	T	-592	23
12	M	R	605	0

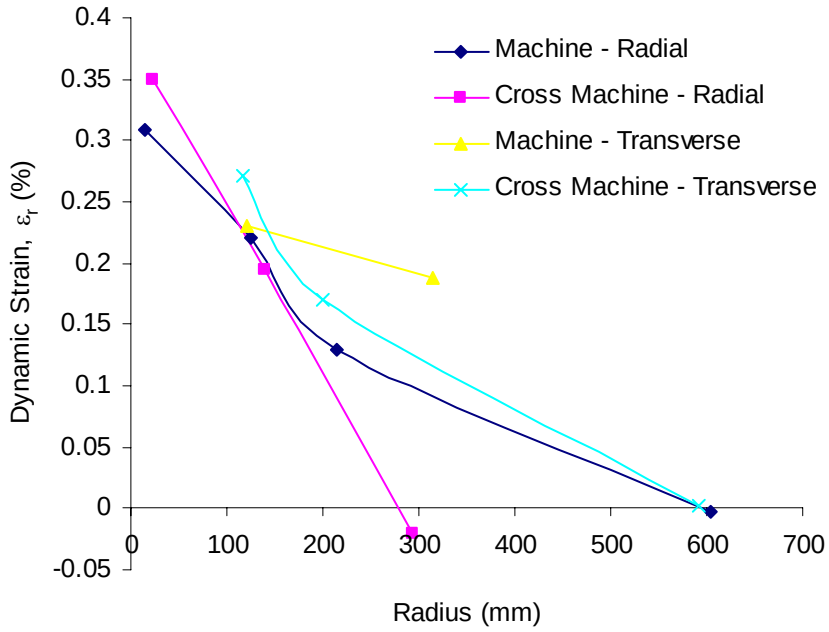

Figure 8: Resilient strain versus radius from the load plate centerline for load cycle 1.

The permanent to resilient strain ratios from all test sections listed in Table 1 subject to the conditions and exceptions described in Table 3 were determined and plotted against the normalized load cycle number and are shown in Figures Figure 9 - Figure 16 by grouping sections having data in the machine or cross machine direction and for MSU sections with geosynthetic A, G or H, (see Table 2 for geosynthetic labels) and for GTX test sections. From this data, the following observations are made:

1. For a given geosynthetic, the curves appear to be similar in shape but are shifted to the left for stronger test sections (i.e., sections with a stronger subgrade, thicker base or the ability to carry more load cycles).
2. The strain ratio appears to be higher for geosynthetics G and H as compared to geosynthetic A and curve upwards more steeply for higher values of $N/N_{25\,mm}$.
3. The curves from the GTX sections appear to be more flat as compared to the curves from the MSU test sections.

The first observation suggests that the curves can be further normalized by shifting the curves horizontally to a common starting point and that the magnitude of the shift will be dependent on the number of load cycles necessary to reach 25 mm of permanent surface deformation ($N_{25\,mm}$). This has been accomplished by computing a shift value (S) taken as the intercept of each curve with the $N/N_{25\,mm}$ axis. This value is determined by computing the slope (in the semi-log plot) of the initial portion of the curve from the first 5 data points and extending this curve backwards until it intersects the $N/N_{25\,mm}$ axis. Each curve is then shifted by this value in order to compute a new normalized load cycle number ($\overline{N}$) computed according to Equation (8), which produces a value of 1 as a starting value when the strain ratio $\varepsilon_p/\varepsilon_r$ is equal to zero (i.e. at cycle 0).

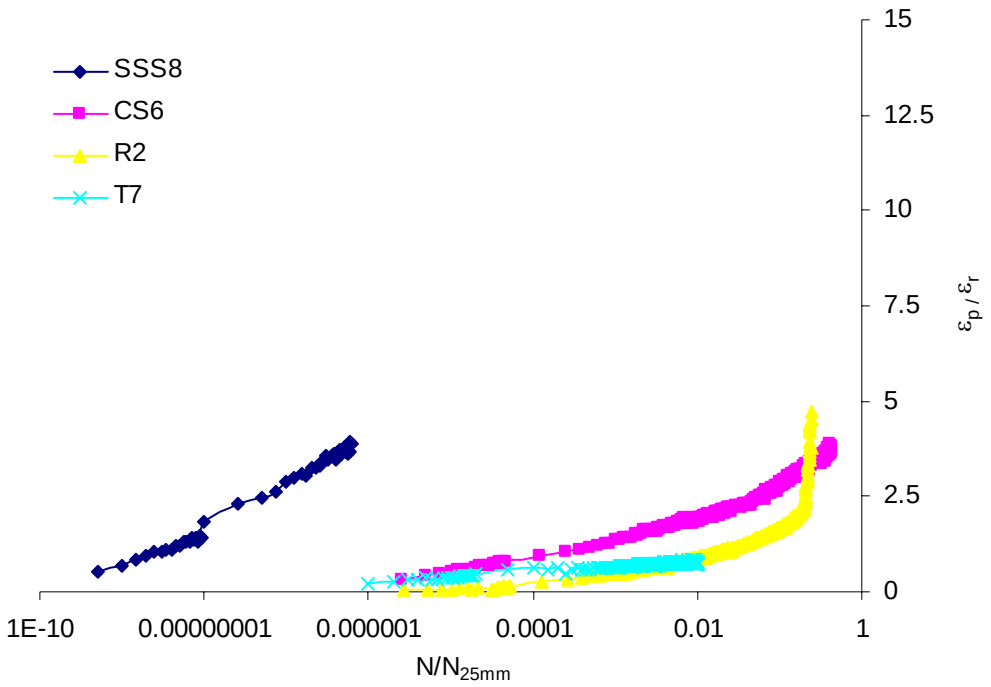

Figure 9: Permanent to resilient strain ratio for MSU test sections with geosynthetic A, machine direction.

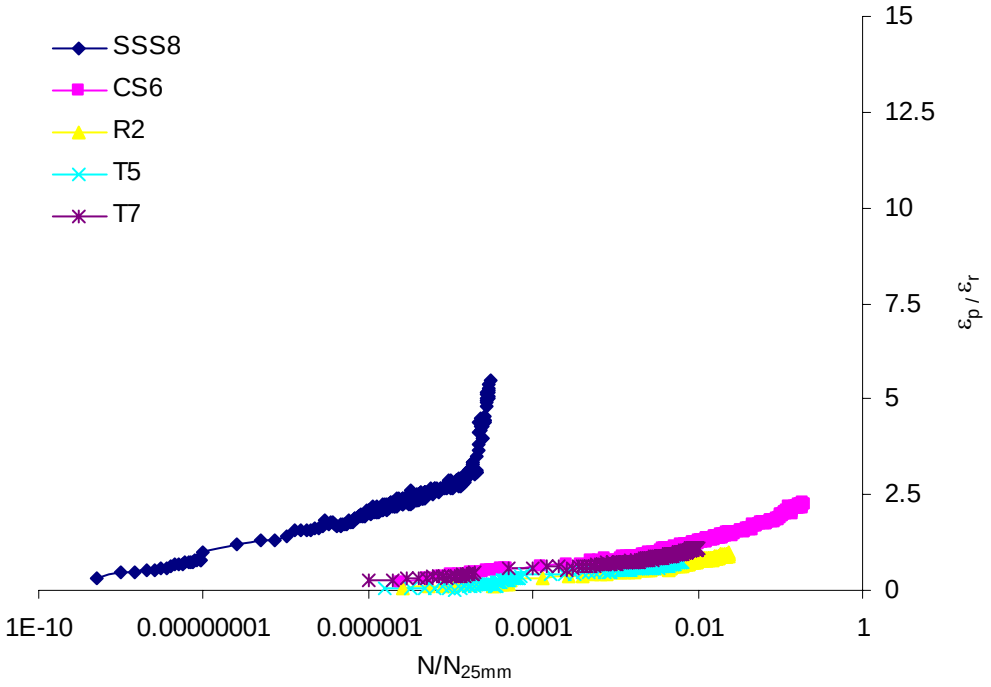

Figure 10: Permanent to resilient strain ratio for MSU test sections with geosynthetic A, cross machine direction.

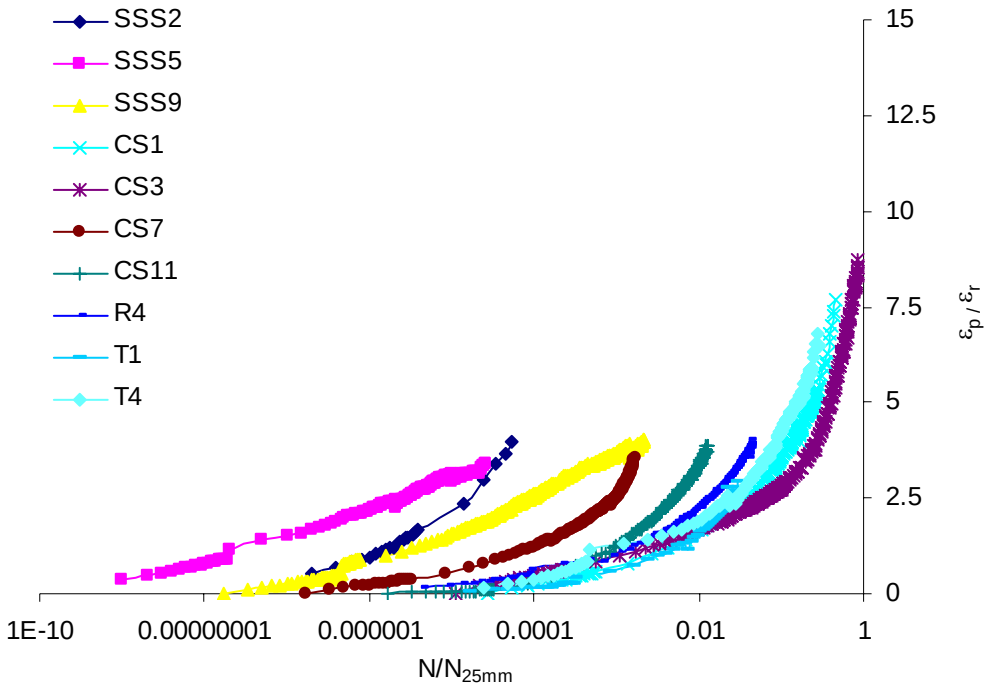

Figure 11: Permanent to resilient strain ratio for MSU test sections with geosynthetic G, machine direction.

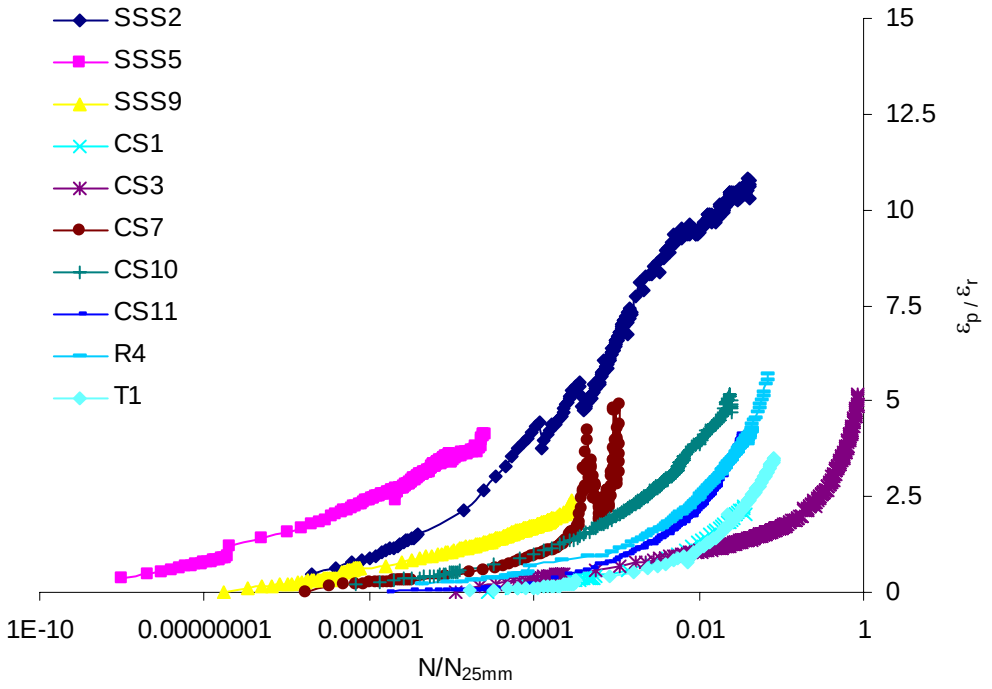

Figure 12: Permanent to resilient strain ratio for MSU test sections with geosynthetic G, cross machine direction.

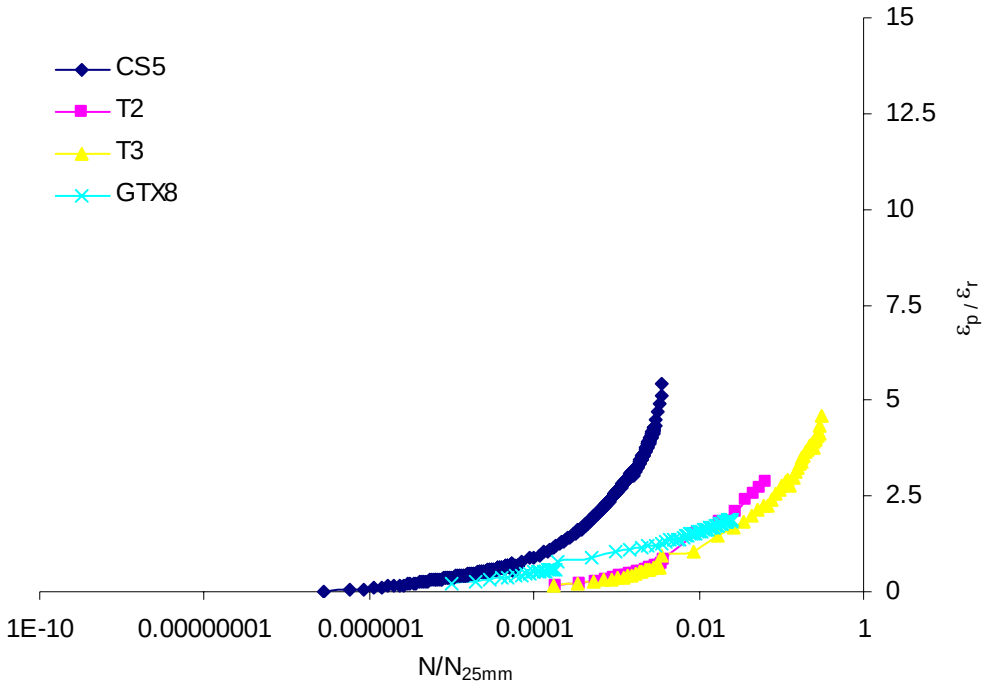

Figure 13: Permanent to resilient strain ratio for MSU test sections with geosynthetic H, machine direction.

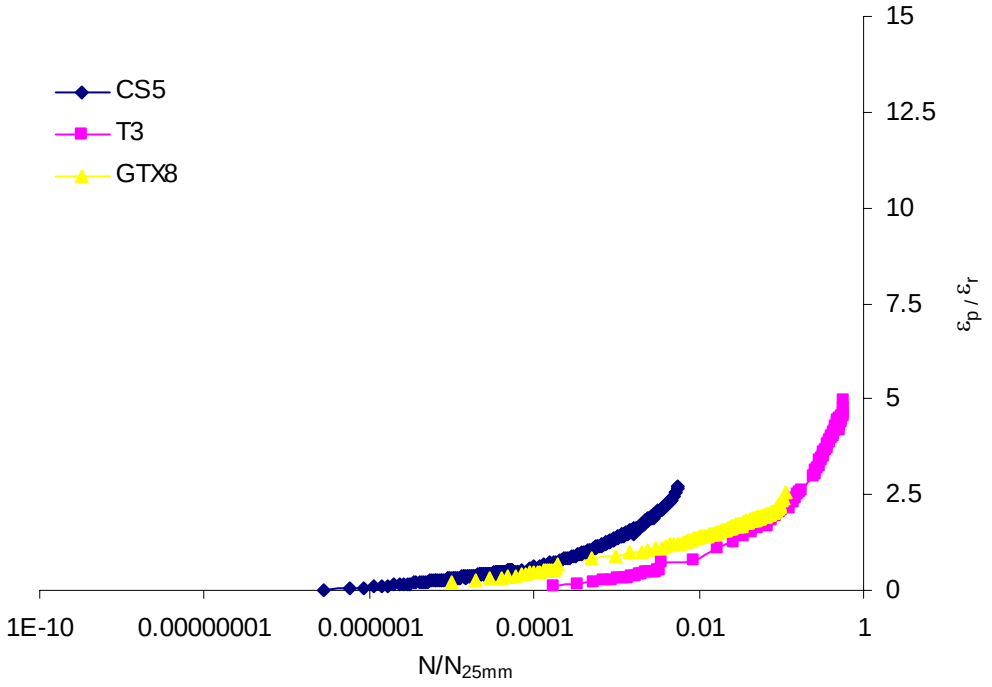

Figure 14: Permanent to resilient strain ratio for MSU test sections with geosynthetic H, cross machine direction.

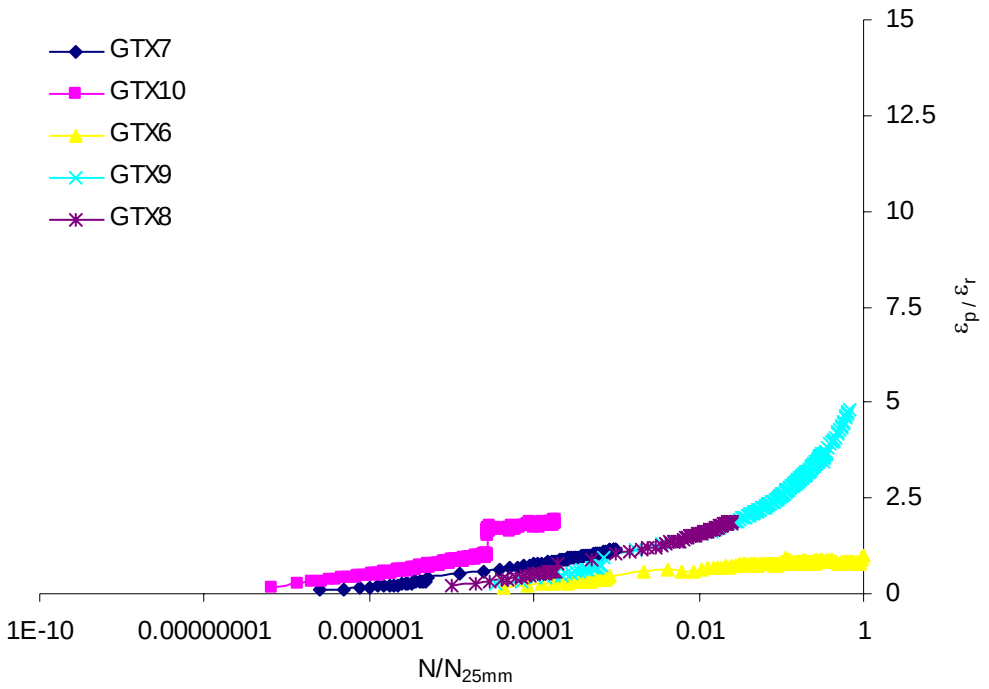

Figure 15: Permanent to resilient strain ratio for GTX test sections, machine direction.

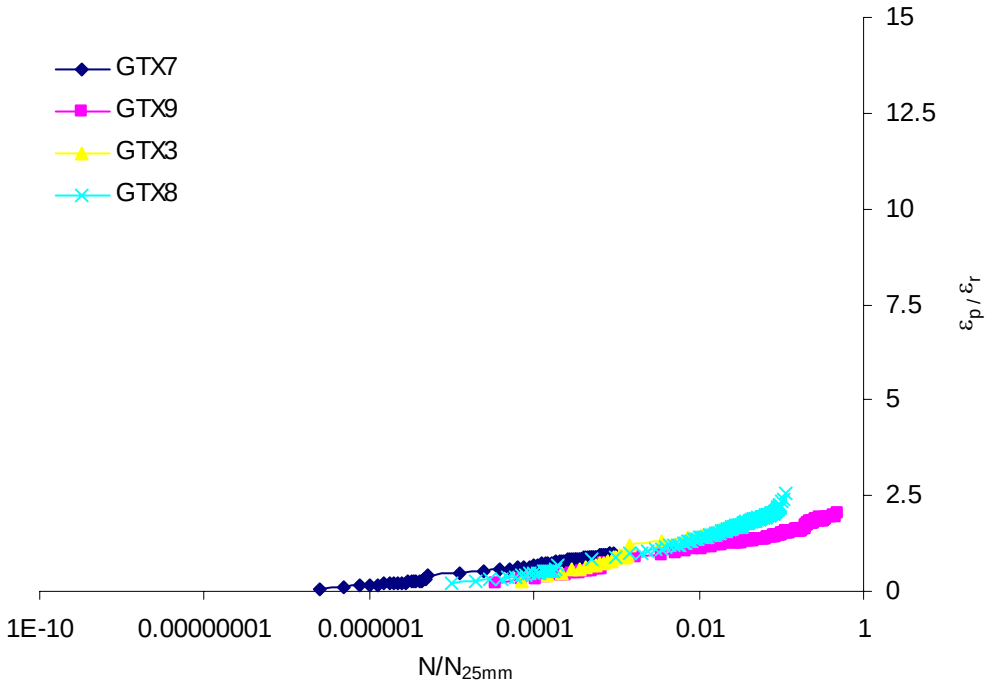

Figure 16: Permanent to resilient strain ratio for GTX test sections, cross machine direction.

$$\overline{N} = 10^{\left(\log\frac{N}{N_{25mm}} - \log S\right)} \tag{8}$$

Values of *S* were tabulated and plotted against $N_{25\ mm}$ for each test section with the results shown in Figure 17. This information indicates that the shift factor can be related to $N_{25\ mm}$ by the Equation (9), where *s* = 1.136. Substituting Equation (9) into (8) results in Equation (10).

$$S = 10^{(-s\log N_{25mm})} \tag{9}$$

$$\overline{N} = 10^{(\log N + (1-s)\log N_{25mm})} \tag{10}$$

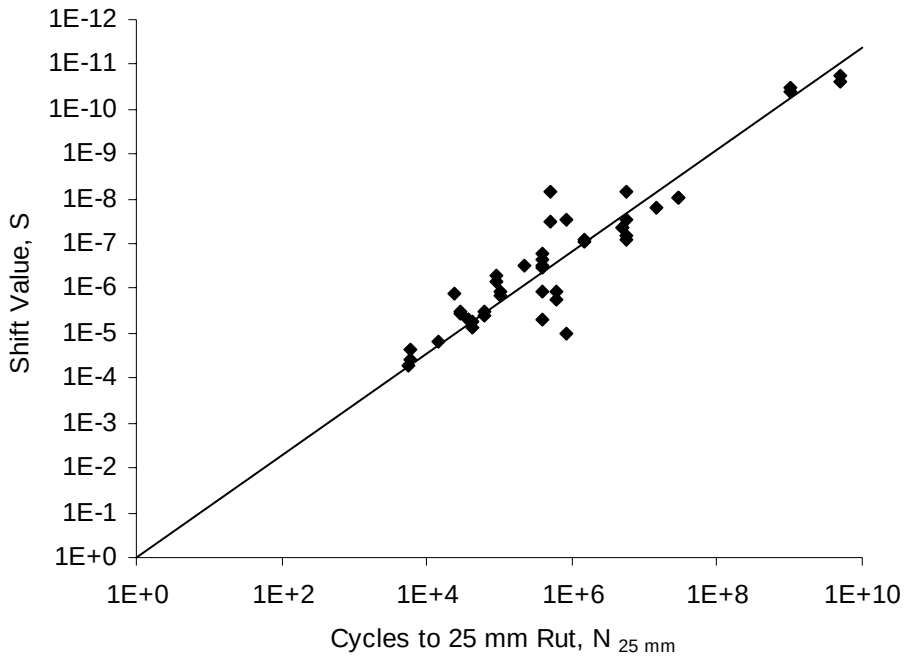

Figure 17: Shift values, S, versus $N_{25\ mm}$ for all test sections.

Figure 25 shows the permanent to resilient strain ratio plotted against $\overline{N}$. From these figures, the following observations are made:

1. Normalizing the data by incorporating the shift value, *S*, allows the curves to be directly compared.
2. No clear trend exists to show a difference in curve shape between the stronger SSS subgrade sections and the weaker CS subgrade. Figures Figure 18 and Figure 19 suggest a steeper curve for section SSS8 as compared to the others. Figures Figure 20 and Figure 21 also show section SSS2 to have a steeper curve, however sections SSS5 and SSS9 show little difference to the other curves.
3. No clear trend exists to show a difference between sections using two aggregate types (CS and T sections as compared to R sections). The R sections contained a rounded pit run aggregate while the CS and T sections contained a crushed aggregate. Figures Figure 18 - Figure 21 show that the R sections are mixed in with the other CS and T sections.

4. No clear trend exists to show differences between the sections containing a reduced aggregate thickness (T sections) and the otherwise identical CS sections. Figures Figure 18 and Figure 19 suggest a less steep curve for sections T5 and T7 as compared to the other CS sections. Figures Figure 20 - Figure 23 do not, however, confirm this trend.
5. The GTX sections appear to show consistently less steep curves than the MSU sections. This may be due to differences in strain gauge mounting techniques and procedures between the two pavement test facilities or may be due to the additional wait period between cycles used in the GTX sections allowing for more stress relaxation in the material.
6. General comparison of curves for geosynthetic A, G and H from the MSU sections show significantly less steep curves for geosynthetic A. Significant differences between geosynthetic G and H are difficult to discern. This is also seen in Figure 25.
7. Figures Figure 24 and Figure 25, confirm less steep curves for the section containing a geotextile (GTX6, geosynthetic D). These figures also tend to suggest differences between the geogrids, with geosynthetics B and C showing less steep curves. These differences appear minor, however, with respect to the data scatter seen in earlier figures.

In general, the data presented in this report suggests that of the variables incorporated in the test sections (geosynthetic type, subgrade strength, aggregate type, aggregate thickness) only geosynthetic type influences the shape of the normalized curve. The shift value of the normalized curve appears to be dependent on the number of load cycles the pavement can carry before reaching 25 mm of permanent surface deformation, which in turn most likely accounts for variables such as subgrade strength, aggregate type and aggregate thickness. Unfortunately, the differences in curve shape between the different geosynthetic types is not as distinct as expected and more work is needed to improve strain measuring techniques to improve this situation.

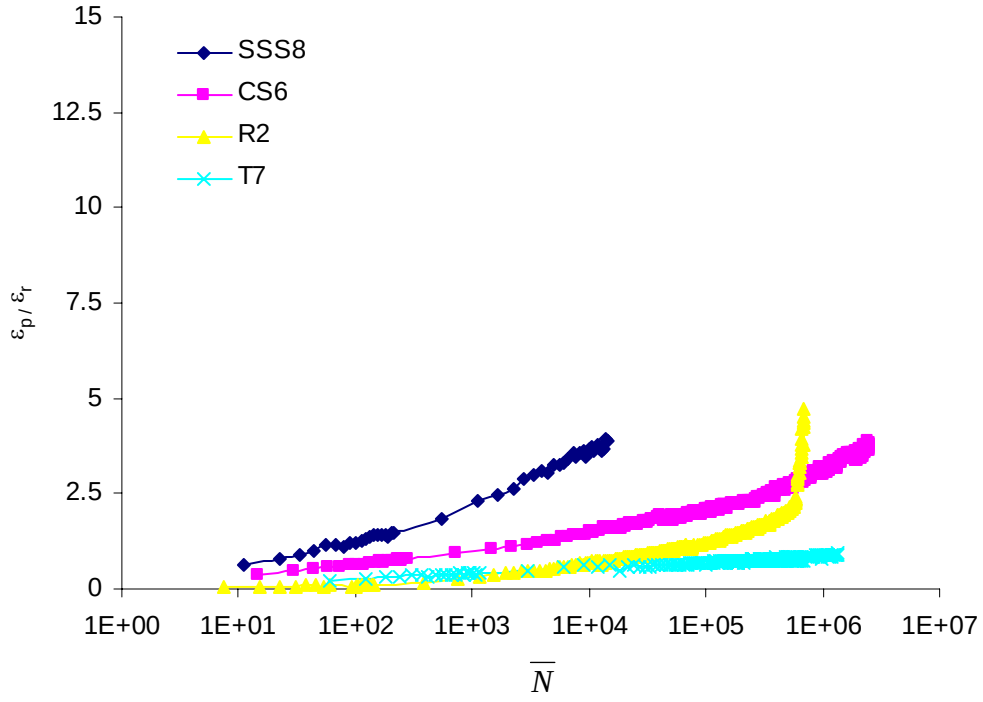

Figure 18: $\varepsilon_p/\varepsilon_r$ versus $\overline{N}$ for MSU test sections with geosynthetic A, machine direction.

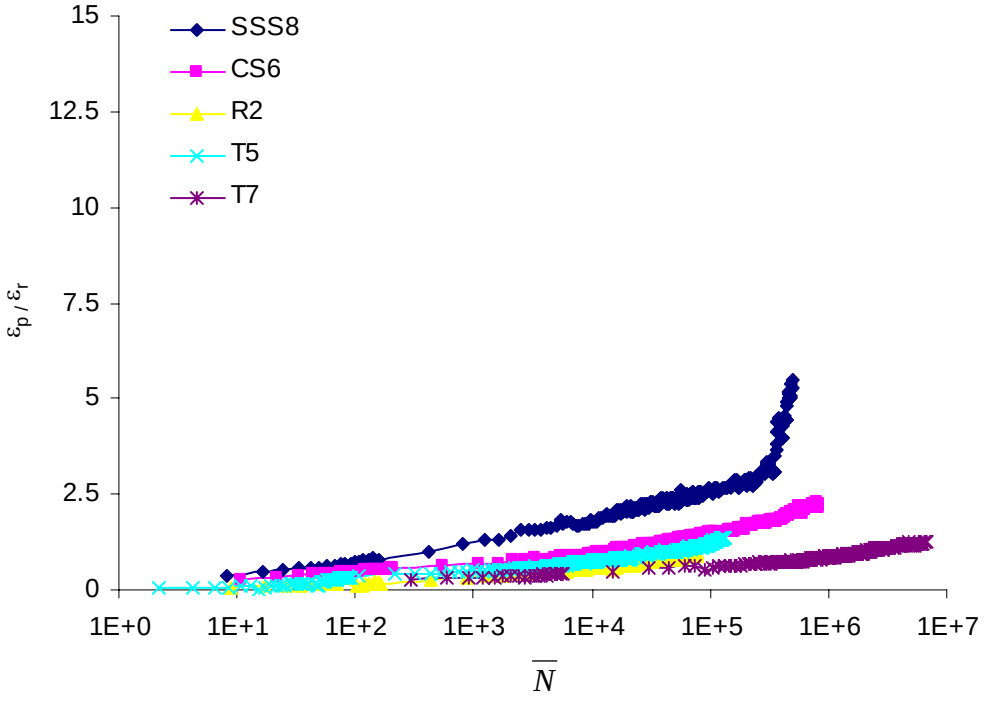

Figure 19: $\varepsilon_p/\varepsilon_r$ versus $\overline{N}$ for MSU test sections with geosynthetic A, cross machine direction.

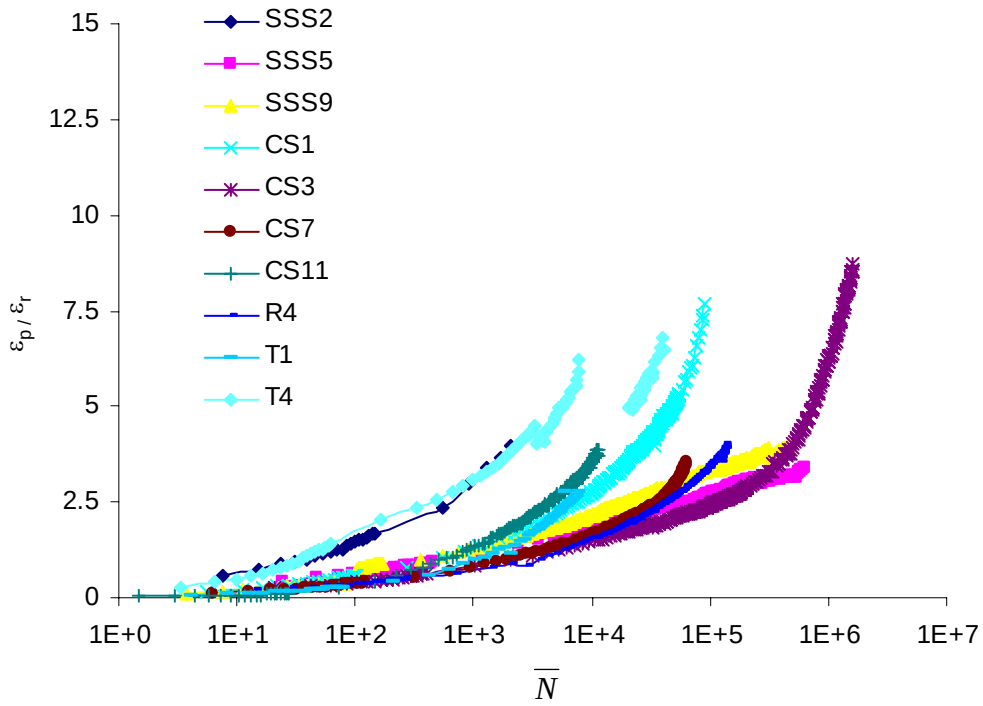

Figure 20: $\varepsilon_p/\varepsilon_r$ versus $\overline{N}$ for MSU test sections with geosynthetic G, machine direction.

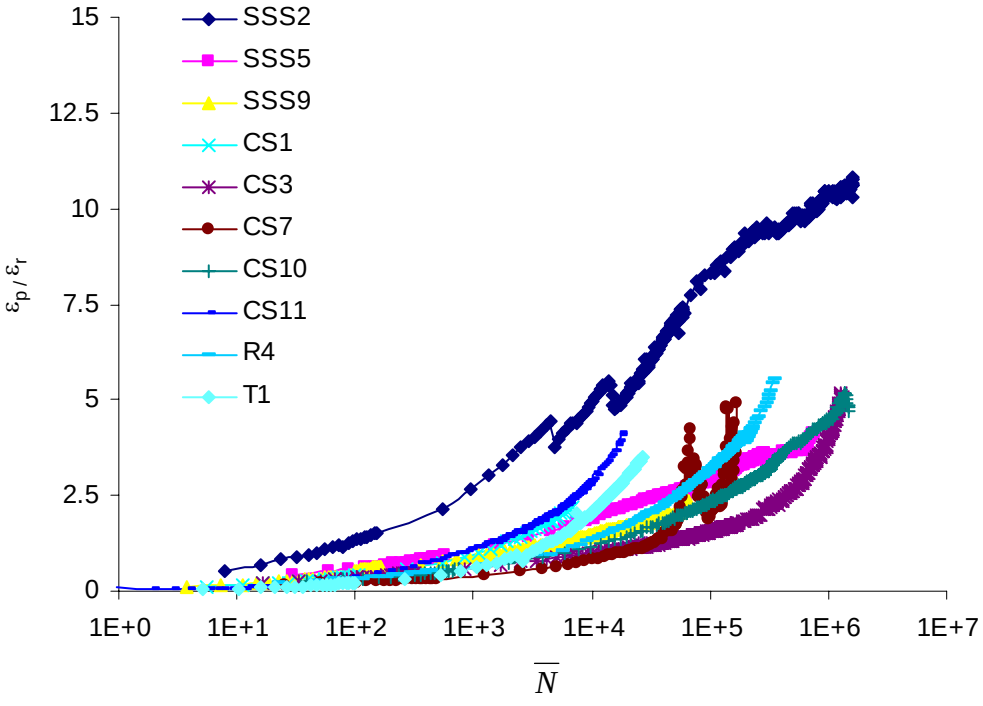

Figure 21: $\varepsilon_p/\varepsilon_r$ versus $\overline{N}$ for MSU test sections with geosynthetic G, cross machine direction.

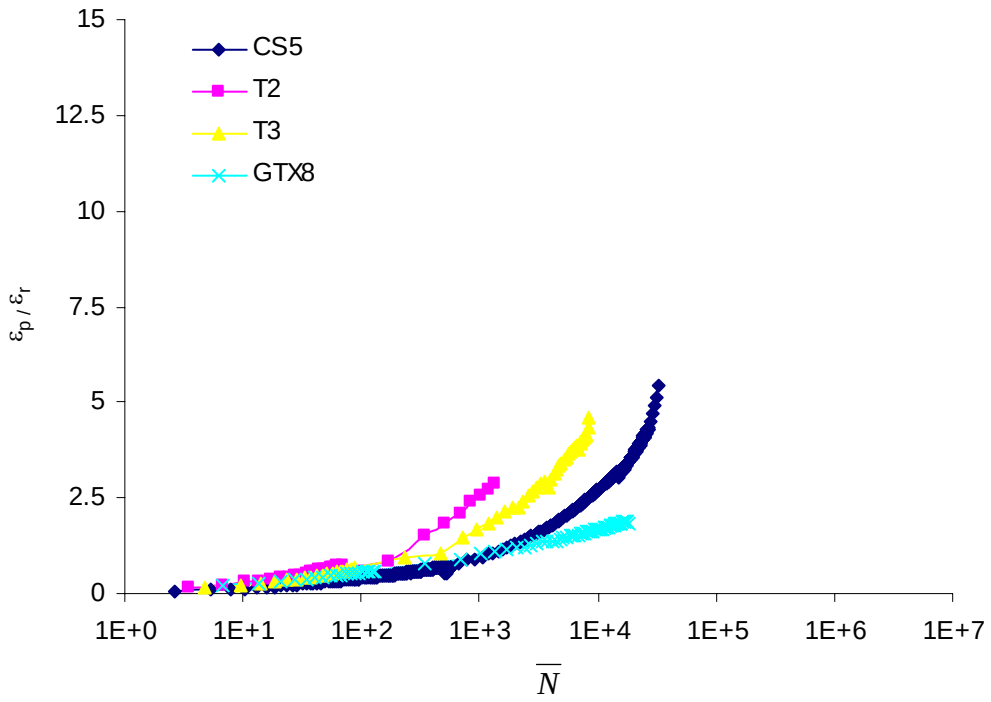

Figure 22: $\varepsilon_p/\varepsilon_r$ versus $\overline{N}$ for MSU test sections with geosynthetic H, machine direction.

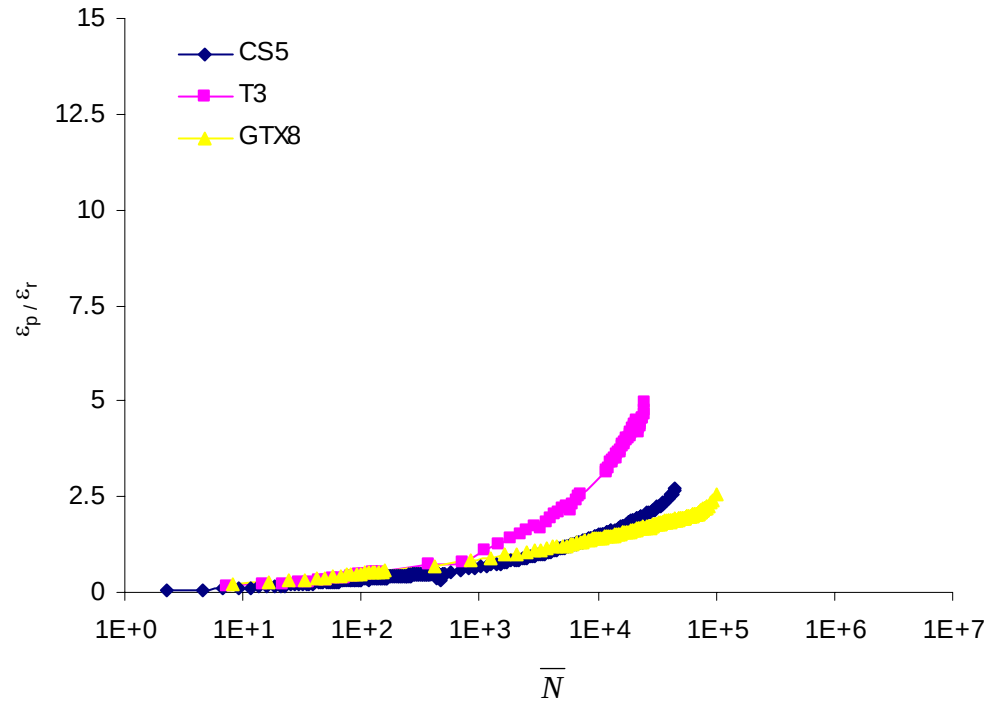

Figure 23: $\varepsilon_p/\varepsilon_r$ versus $\overline{N}$ for MSU test sections with geosynthetic H, cross machine direction.

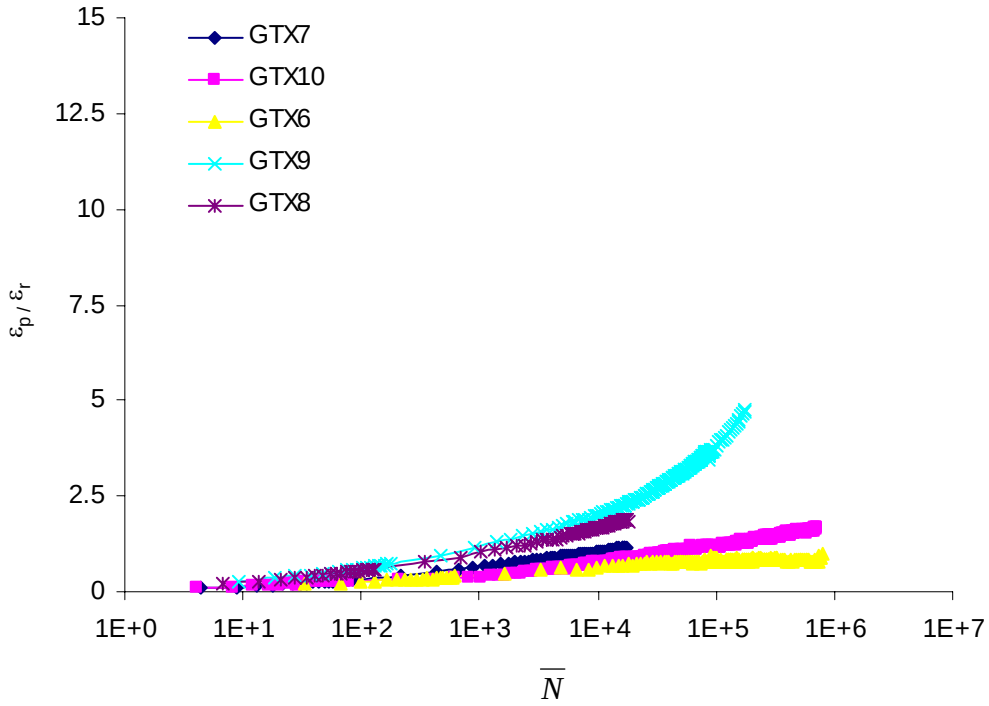

Figure 24: $\varepsilon_p/\varepsilon_r$ versus $\overline{N}$ for GTX test sections, machine direction.

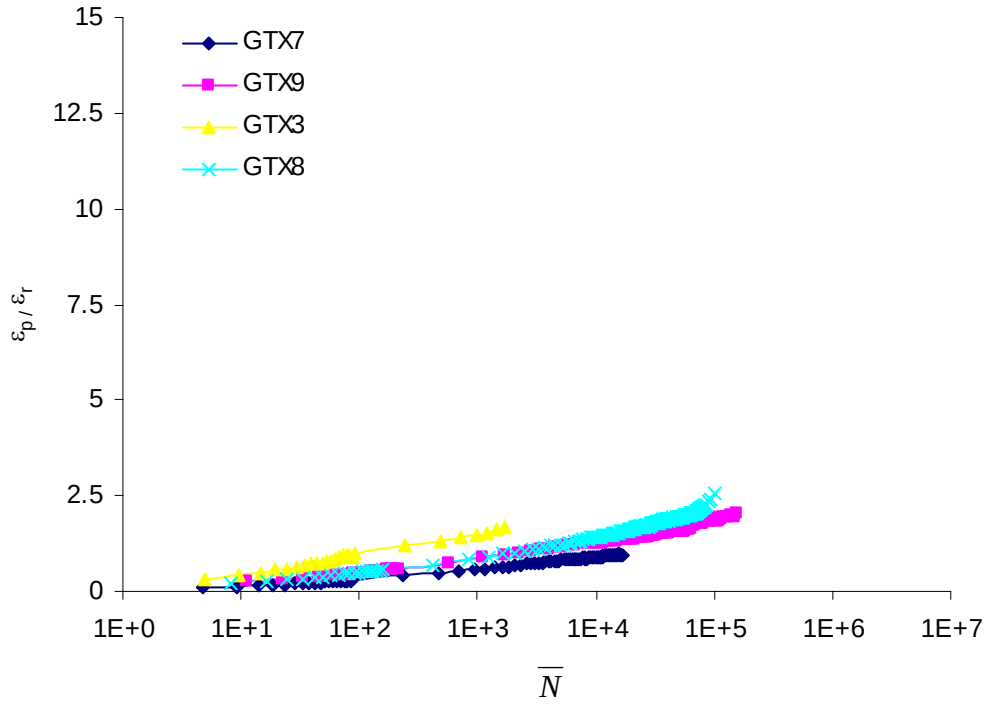

Figure 25: $\varepsilon_p/\varepsilon_r$ versus $\overline{N}$ for GTX test sections, cross machine direction.

5. RECOMMENDATIONS AND ANTICIPATED USE

The curves shown in Figures Figure 18 - Figure 25 can be described by Equation (11), where *A* and *B* are curve fitting parameters. The normalized load cycle number, $\overline{N}$, was defined previously and is given again by Equation (10), where s = 1.136, N = number of applied load cycles, and N_{25mm} = the number of load cycles necessary to reach 25 mm of permanent surface deformation. The above work suggests that the parameters *A* and *B* are functions of the geosynthetic type, however further work is needed to fully establish this.

$$\log\left(\frac{\varepsilon_p}{\varepsilon_r}\right) = \log A + B\log\overline{N} \tag{11}$$

$$\overline{N} = 10^{(\log N + (1-s)\log N_{25mm})} \tag{12}$$

Earlier work (Perkins et al., 2004) used an equation similar in form to Equation (11) where the strain ratio was also dependent on N and N_{25mm}. This previous equation used the ratio of N/N_{25mm}, however, which has a terminal value of 1 when $N = N_{25mm}$, meaning that the terminal value of the strain ratio could be calculated without the need to know the value of N_{25mm}. The procedure used by Perkins et al. (2004) was then to select approximately 5 values of permanent strain ratio with the last value being the terminal value and using these values in Equation (7) to evaluate the effects of shear restraint on the pavement section for various periods of pavement life. The procedure needed when using Equations (10) and (11) will be different in that a terminal value of strain ratio will not be initially known since the value of N_{25mm} will not be initially known. This may require the analysis of additional periods corresponding to additional values of the strain ratio until the predicted pavement life corresponds to the assumed value of N_{25mm}. With these changes, the new relationships described above can otherwise be directly used in the procedures described in Perkins et al. (2004).

The most obvious need seen from the work described in this report is a reliable means of determining parameters *A* and *B* in Equation (11). Given the data scatter seen in the above results, it is unclear if the construction of additional test sections is the best approach. Improvements in strain gauging techniques or the use of other novel strain measuring devices could improve this situation and allow experimental curves to be extended further into the loading life of the pavement (many gauges failed prematurely). It is anticipated that the development of reliable data allowing for discernable differences to be seen between geosynthetics would then allow parameters *A* and *B* to be empirically related to geosynthetic and interface properties.

6. REFERENCES

NCHRP (2004), *NCHRP Project 1-37 Design Guide: Mechanistic-Empirical Design of New and Rehabilitated Pavement Structures*, http://www.trb.org/mepdg/guide.htm.

Perkins, S.W. (2002), *Evaluation of Geosynthetic Reinforced Flexible Pavement Systems Using Two Pavement Test Facilities*, Montana Department of Transportation, Helena, MT and the U.S. Department of Transportation, Federal Highway Administration, Washington, DC, Report No. FHWA/MT-02-008/20040, 120 p.

Perkins, S.W. (1999), *Geosynthetic Reinforcement of Flexible Pavements: Laboratory Based Pavement Test Sections*, Montana Department of Transportation, Helena, MT and the U.S. Department of Transportation, Federal Highway Administration, Washington, DC, Report No. FHWA/MT-99/8106-1, 140 p.

Perkins, S.W., Christopher, B.R., Cuelho, E.L., Eiksund, G.R., Hoff, I., Schwartz, C.W., Svanø, G., and Watn, A., (2004) *Development of Design Methods for Geosynthetic Reinforced Flexible Pavements*, U.S. Department of Transportation, Federal Highway Administration, Washington, DC, FHWA Report Reference Number DTFH61-01-X-00068, 263p.